Cross-equatorial structure and temporal modulation of intraseasonal variability at the surface of the Tropical Atlantic Ocean

Le Gos, Gabriela Athie, Frédéric Marin

Cross-equatorial structure and temporal modulation of intraseasonal variability at the surface of the Tropical Atlantic Ocean

Gabriela Athie[1] and Frédéric Marin[1]

Received 10 May 2007; revised 4 April 2008; accepted 14 April 2008; published 12 August 2008.

[1] Intraseasonal variability (10–50 days) in the equatorial Atlantic Ocean is analyzed from multiyear (1999–2005) satellite gridded products of sea-level anomalies (SLA) and sea-surface temperature (SST). Two regions with distinct intraseasonal variability have been identified. The first one, west of 10°W, is dominated by westward-propagating anomalies, with maximum values in SLA along 5°N and in SST along 2°N: They occur in boreal summer with periods of 25–50 days and are known to correspond to tropical instability waves (TIWs). We show that TIWs have also a signature, though weaker, south of the equator, especially along 5°S, in SLA. Northern and southern anomalies propagate together westward, being mostly out of phase, suggesting that equatorial wave dynamics is involved in TIWs variability. An SST signature of TIWs is also observed near 2°S, in quadrature with SST anomalies detected in the Northern Hemisphere. The interannual modulations of the TIW signature in SLA and SST are compared and discussed. The second dominant intraseasonal signal is only seen east of 10°W in SST and corresponds to an equatorially trapped variability, confined to the Gulf of Guinea with periods between 10 and 20 days. This signal is present in boreal summer when an intense SST front is observed just north of the equator. Intraseasonal variability with comparable periods is also observed in the meridional wind stress throughout the year. Comparison of SST and meridional wind stress anomalies suggests that the 10- to 20-day variability in SST is forced by the wind stress but seasonally modulated by the presence of the SST front.

Citation: Athie, G., and F. Marin (2008), Cross-equatorial structure and temporal modulation of intraseasonal variability at the surface of the Tropical Atlantic Ocean, *J. Geophys. Res.*, *113*, C08020, doi:10.1029/2007JC004332.

1. Introduction

[2] Equatorial oceans are the location of strong zonal currents and act as waveguides that quickly respond to temporal variability in the forcing. Two different sources of intraseasonal variability (defined in the present paper as periods between 10 and 50 days) are present in the equatorial Atlantic Ocean. The first one results from tropical instabilities and is mainly observed at periods between 15 and 50 days [*Qiao and Weisberg*, 1995; *Jochum et al.*, 2004]. The second one is directly forced by intraseasonal variability in the winds and is maximum at periods close to 15 days [e.g., *Houghton and Colin*, 1987; *Garzoli*, 1987].

[3] Tropical instability waves (TIWs) have their strongest signature at the surface in the Northern Hemisphere. They are observed along 5°N in sea-level anomalies as intense mesoscale structures (Figure 1a), associated with undulations of the seasonal sea-surface temperature (SST) front (Figure 1b) that delimits the cold tongue in boreal summer [*Chelton et al.*, 2001; *Hashizume et al.*, 2001; *Caltabiano et al.*, 2005; *Foltz et al.*, 2004]. TIWs are described from observations as propagating westward with phase velocities between 30 and 60 cm/s, periods ranging from 15 to 50 days and wavelengths close to 1000 km [*Steger and Carton*, 1991; *Qiao and Weisberg*, 1995; *Caltabiano et al.*, 2005]. Subsurface observations of currents [*Düing et al.*, 1975; *Brandt et al.*, 2006; *Bunge et al.*, 2006] and temperature [*Wainer et al.*, 2003] reveal that TIWs are not confined to the near-surface layers, but are still present within and beneath the thermocline. In situ observations [*Weisberg and Weingartner*, 1988; *Grodsky et al.*, 2005] and numerical models [*Jochum et al.*, 2004; *Jochum and Murtugudde*, 2006; *Peter et al.*, 2006] indicate that TIWs are a major source of heat for the equatorial mixed layer and lead to important heat and/or momentum transfers between the mixed layer and the underlying ocean. The SST signature of TIWs is finally found to be associated with westward-propagating atmospheric structures of the same temporal and spatial scale [e.g., *Hashizume et al.*, 2001], that may interact with the Intertropical Convergence Zone at interannual timescales [*Caltabiano et al.*, 2005].

[4] TIWs are common to both Atlantic and Pacific oceans [*Chelton et al.*, 2000] where they are forced by complex mechanisms involving oceanic instabilities. They can first be generated by barotropic instability of the meridional shear of seasonally varying zonal currents [*Philander*, 1976, 1978], either at the surface (between the South Equatorial Current, SEC and the North Equatorial Countercurrent, NECC) or within the thermocline (between the SEC and the Equatorial

[1] LEGOS-UMR, CNRS/CNES/IRD/UPS, Centre IRD de Bretagne, Plouzané, France.

0148-0227/08/2007JC004332

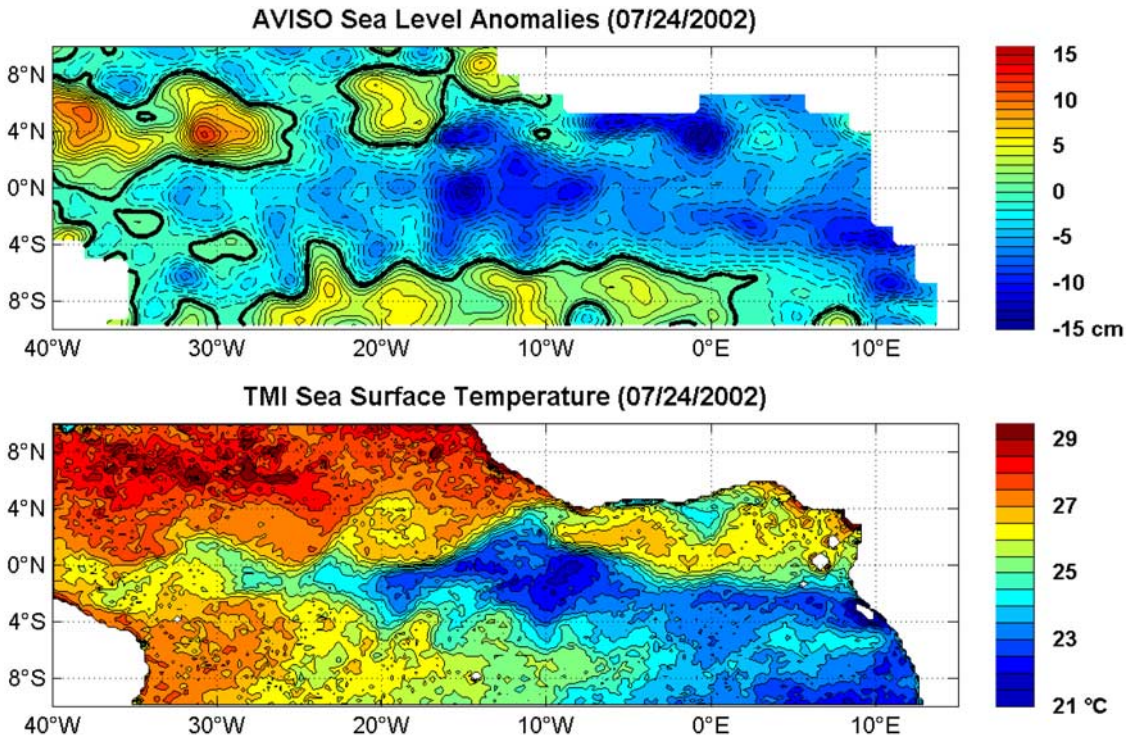

Figure 1. Surface distribution of (top) AVISO sea-level anomalies (in centimeters) and (bottom) TMI sea-surface temperature (in degrees centigrade) in the equatorial Atlantic in 24 July 2002. Interval between contours is 1 cm for SLA and 0.5°C for SST. Negative values in SLA are in dashed line.

Undercurrent, EUC) [*Qiao and Weisberg*, 1998]. They can also originate from baroclinic instability of the equatorial upwelling front or of the meridionally shoaling thermocline [*Yu et al.*, 1995]. In the Atlantic Ocean, observations [*Grodsky et al.*, 2005] and numerical studies [*Jochum et al.*, 2004] suggest that barotropic and baroclinic instabilities both contribute to the formation of TIWs.

[5] There is no consensus about the exact nature of TIWs in the equatorial Atlantic. They can be first seen as three-dimensional vortices advected westward along 5°N by equatorial surface currents [*Menkès et al.*, 2002; *Foltz et al.*, 2004]. They can also be explained in terms of equatorial waves, either as Rossby waves with periods greater than 30 days along 5°N [*Jochum and Malanotte-Rizzoli*, 2003] or as mixed Rossby-gravity waves closer to the equator, where they are observed below the surface from current meters with periods extending from 15 to 40 days [*Düing et al.*, 1975; *Weisberg et al.*, 1979].

[6] Undulations of the SST front are not restricted to the Northern Hemisphere, but are also observed south of the equator in the center of the basin in July 2002 (Figure 1b). Such features were previously evidenced from satellite SST observations [*Steger and Carton*, 1991; *Chelton et al.*, 2000; *Bunge et al.*, 2006], and referred to as TIWs. However, the precise characteristics of this southern intraseasonal variability still need to be documented in the Atlantic. *Steger and Carton* [1991] and *Bunge et al.* [2007] could not find any clear relation between the northern and southern TIW signatures in SST, suggesting that TIWs north and south of the equator do not have the same dynamical origin. In contrast, in the Pacific Ocean, *Lyman et al.* [2005, 2007] relate together the northern and southern signatures of TIWs as the interhemispheric manifestation of equatorial waves. The weaker amplitudes south of the equator result in that case from the deformation of theoretical equatorial waves due to the latitudinal structure of background zonal currents (especially the presence of the NECC north of the equator).

[7] SST observations show a significant interannual variability in TIW activity [*Steger and Carton*, 1991; *Contreras*, 2002; *Caltabiano et al.*, 2005]. *Wu and Bowman* [2007] relate the year-to-year modulation in the amplitude of the TIWs SST variance to the intensity of the equatorial cold tongue. Moreover, *Caltabiano et al.* [2005] suggest that TIWs have larger wavelengths and faster phase speeds during years of stronger equatorial upwelling, while the period and position of TIWs maximum depend essentially on the timing of the seasonal equatorial cold tongue. However, it is difficult to conclude from SST observations alone about the interannual variability of the TIWs themselves, since the temporal variability of the TIWs signature in SST reflects changes in dynamics as well as in the background temperature gradient that is required for TIWs to have a signature in SST.

[8] The 10- to 20-day variability at the surface of the Tropical Atlantic Ocean has been less studied than TIWs, though this signal is an important contributor to the cooling of the mixed layer during the seasonal upwelling in the Gulf of Guinea [*Houghton and Colin*, 1987]. This signal has been observed at the surface and subsurface from temperature and velocity data records [*Garzoli*, 1987; *Bunge et al.*, 2006], but also in the atmosphere from wind stress data records [*Houghton and Colin*, 1987; *Mounier et al.*, 2008]. At intraseasonal scales, the most energetic peak

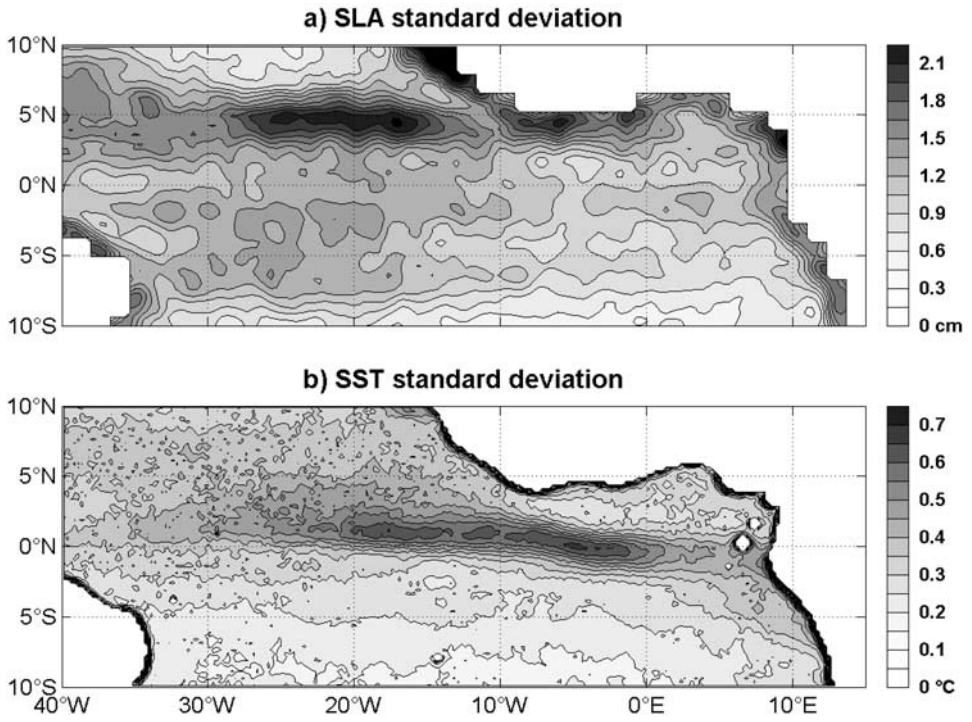

Figure 2. Horizontal distribution of standard deviation of 10- to 50-day filtered anomalies in (a) SLA (in centimeters) and in (b) SST (in degrees centigrade, lower) over the period 1999–2005.

in the meridional wind is centered at 14 days in the tropical Atlantic and is significantly correlated with meridional velocity, suggesting a dominant forcing by the wind [*Garzoli*, 1987]. Comparing current velocity, wind stress and in situ temperature data within the 10- to 20-day frequency band, *Houghton and Colin* [1987] found that this variability was present all along the year in the meridional wind stress and current velocity. This variability was related to a mixed Rossby-gravity wave, on the basis of the observation that the thermocline vertical displacement was antisymmetric with respect to the equator [*Houghton and Colin*, 1987].

[9] The goal of this paper is to analyze the spatial structure and temporal modulation of the intraseasonal

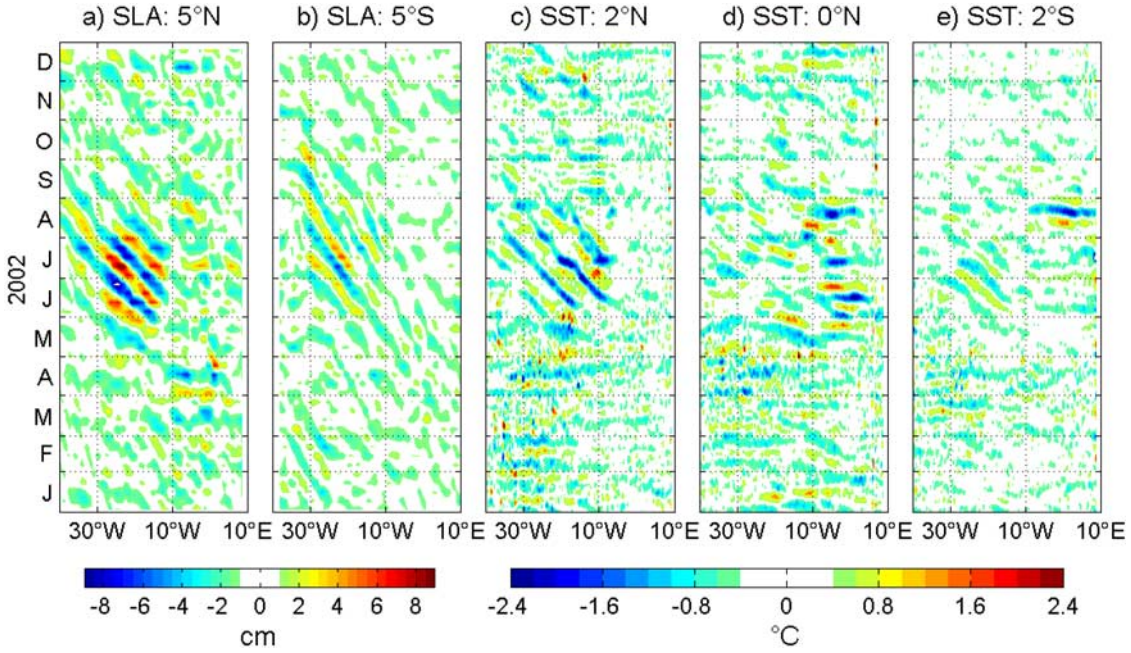

Figure 3. Time-Longitude plot of intraseasonal anomalies (<50 days) in 2002. SLA anomalies along (a) 5°N and along (b) 5°S and SST anomalies along (c) 2°N, (d) the equator, and (e) 2°S.

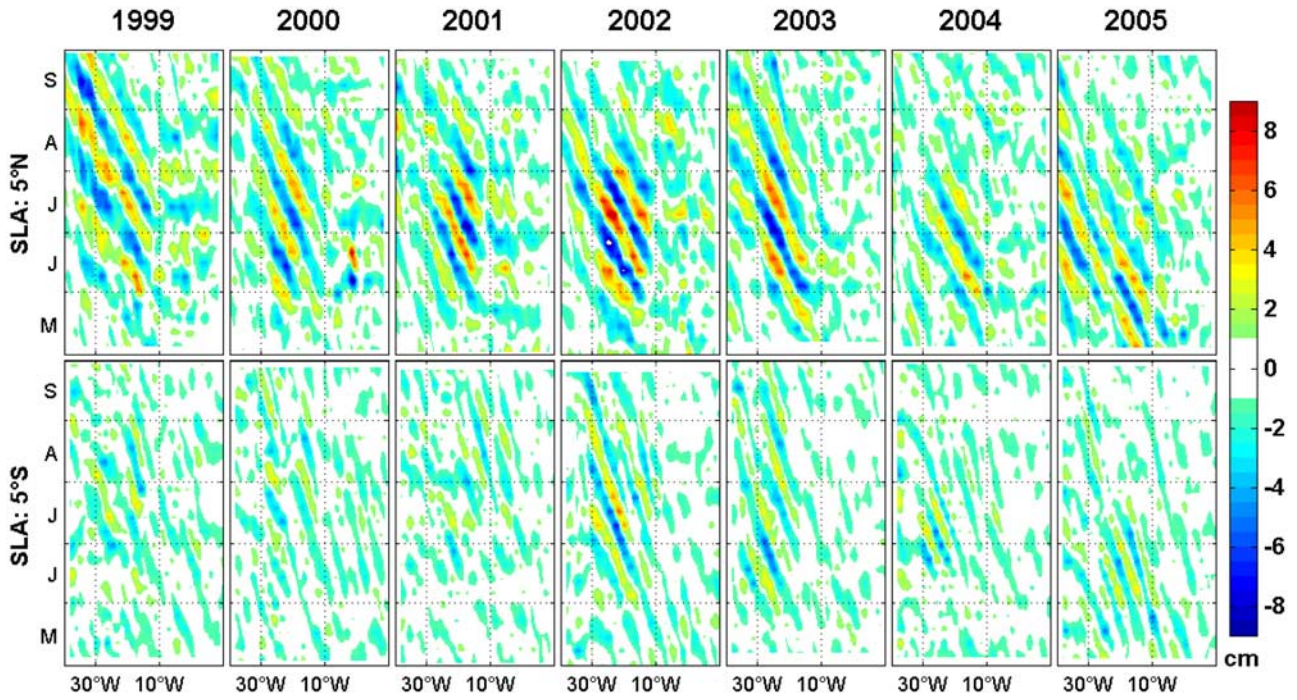

Figure 4. Time-Longitude plot of SLA intraseasonal anomalies (<50 days) from 1 May to 30 September for every year (from 1999 to 2005), along (top) 5°N and (bottom) 5°S.

variability at periods between 10 and 50 days in the equatorial Atlantic Ocean from multiyear satellite observations of SLA and SST. The data and methods of analysis are presented in section 2. Section 3 describes the dominant patterns of intraseasonal variability. The mean properties of TIWs, their interannual variability and seasonal evolution are discussed in section 4. Section 5 focuses on the 10- to 20-day variability. Finally results are discussed and summarized in section 6.

2. Data

2.1. SLA and SST data

[10] In this study the surface signature of intraseasonal variability is analyzed from satellite observations of SST and SLA for the period 1999–2005.

[11] We use the SLA gridded product distributed by AVISO, with a 7-day temporal resolution and 1/3° spatial resolution. This data set was generated using objective analysis to combine information from several satellites by Ssalto/Duacs (Segment Sol multimissions d'ALTimétrie, d'Orbitographie et de localisation precise/Developing Use of Altimetry for Climate Studies) (http://www.jason.oceanobs.com).

[12] For SST data we use a gridded product, distributed by Remote Sensing Systems (http://www.remss.com), of the Tropical Rainfall Measuring Mission Microwave Imager (TMI) sensor. TMI is a nine-channel passive microwave radiometer with operating frequencies ranging from 10.65 to 85.5 GHz [*Kummerow et al.*, 1998]. The lowest-frequency channel of this radiometer yields SST images even in the presence of non-rain clouds, in contrast to infrared radiometers that require cloud-free conditions. However, it is sensitive to rain conditions. TMI data are available every day as 3-day running averages with a spatial resolution of 0.25 degrees in latitude and longitude. Data have been linearly interpolated in time to fill gaps due to rain.

[13] *Chelton et al.* [2001] validated TMI data at the temporal and spatial scales of the TIWs over the Pacific through the comparison with *in situ* data from the Tropical Atmospheric – Ocean Project (TAO) during 1999. The authors found that possible systematic errors in TMI data did not alter significantly observations of TIWs. Since intraseasonal variability has similar scales in the Atlantic and in the Pacific, we assume that their results still hold in the Atlantic.

2.2. Complementary Data

[14] The properties derived from SST and SLA satellite observations were compared to other satellite-derived products for the whole period 2000–2005 to study the possible mechanisms of temporal modulation of the intraseasonal variability.

[15] Surface wind stress was studied using the daily QuikSCAT gridded product distributed by CERSAT. Its horizontal resolution is 0.5 degrees and this product is available from January 2000 (http://www.ifremer.fr/cersat/en/data/overview/gridded/mwfqscat.htm).

[16] Oceanic surface currents were analyzed using the gridded product of surface velocities computed from the Ocean Surface Current Analyses Real-Time (OSCAR) model [*Bonjean and Lagerloef*, 2002]. This model provides diagnostic ocean surface velocity fields from the combination of SLA data, SSM/I + QUIKSCAT winds and Reynolds SST with a temporal resolution of 5 days and a spatial resolution of 1 degree. It is based on the quasi-steady and

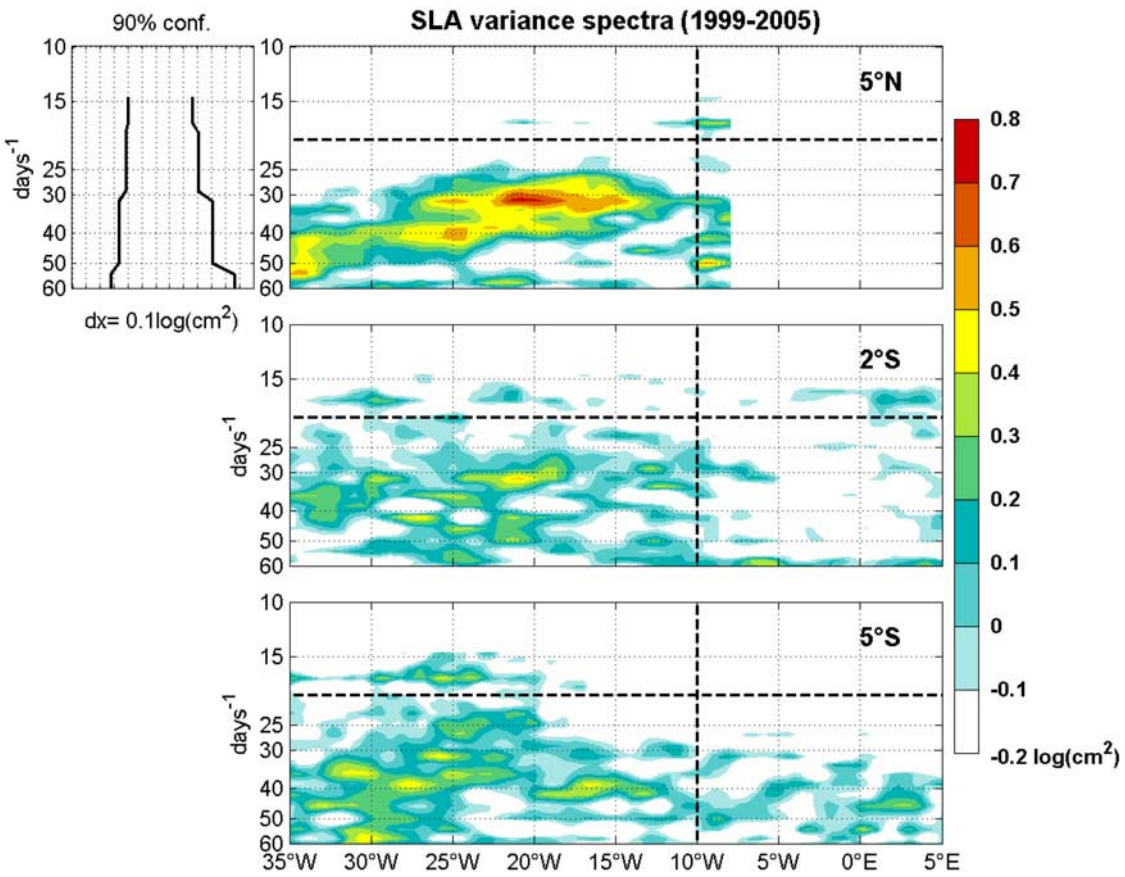

Figure 5. Longitudinal distribution of the variance spectra of SLA along (top) 5°N, (middle) 2°S, and (bottom) 5°S with respect to frequency (in logarithmic scale). Contour interval is 0.1 log(cm^2). Dashed lines refer to the 10°W longitude (vertical line) and to the 20-day period (horizontal line). The 90% confidence interval is 0.65 log(cm^2) for 30–50 days, 0.5 log(cm^2) for 18–30 days, and 0.45 log(cm^2) for 14–18 days. Variances are normalized by the zonally averaged variance for the corresponding 10- to 50-day anomalies, namely, 3.1 cm^2 at 5°N, 1.6 cm^2 at 2°S, and 1.3 cm^2 at 5°N.

quasi-linear equations of the flow and on the optimization of a horizontal momentum balance near the equator. The resulting velocities were validated with observational data from buoy drifters and current meters in the Pacific Ocean. The velocity error was estimated to be 8 cm/s for zonal mean flow and 3 cm/s for meridional mean flow [*Bonjean and Lagerloef*, 2002].

2.3. Methodology

[17] A Lanczos filter [*Emery and Thomson*, 2004] was applied in time to SST and SLA data to compute both intraseasonal anomalies (between 10 and 50 days) and low-frequency variability (periods greater than 50 days). The Lanczos filter was applied over 183 days for both data sets, which corresponds to 183 time points in SST and 27 time points in SLA. Unlike *Caltabiano et al.* [2005] who only looked at westward-propagating anomalies, we performed here no filtering in longitude to keep the full (propagating and nonpropagating) 10- to 50-day variability.

[18] The energy spectra of SST and SLA time series were estimated using the fast Fourier transform (FFT) to identify the dominant periods of intraseasonal variability. Energy in specific frequency bands was averaged to increase the degrees of freedom, which are between 10 and 20 for the frequencies corresponding to the intraseasonal timescales (10–50 days).

[19] In section 3.2 we perform an Hilbert Complex Empirical Orthogonal Function Analysis (CEOF) as defined in details in *Barnett* [1983]. This method separates the variability of the signal in orthogonal modes which are composed of a spatial part (empirical function) and a temporal one (principal component). Unlike EOF, the CEOF takes into account the propagation of the signal and thus allows us to estimate the amplitude and phase of the spatial and temporal complex parts.

3. General Characteristics of the Intraseasonal Signal

3.1. Spatial Distribution of Maximum Variability

[20] Standard deviation maps of SLA and SST intraseasonal anomalies (10–50 days) are presented in Figure 2 to stress regions of maximum variability. The largest standard deviation of SLA anomalies (~2.1 cm, within the confidence interval 1.7–2.7 cm) are located along 5°N in the middle of the basin, between 30°W and 10°W (Figure 2a) and correspond to TIWs. Moreover standard deviation around 1.5 cm (confidence interval of 1.3–1.8 cm) is observed in the

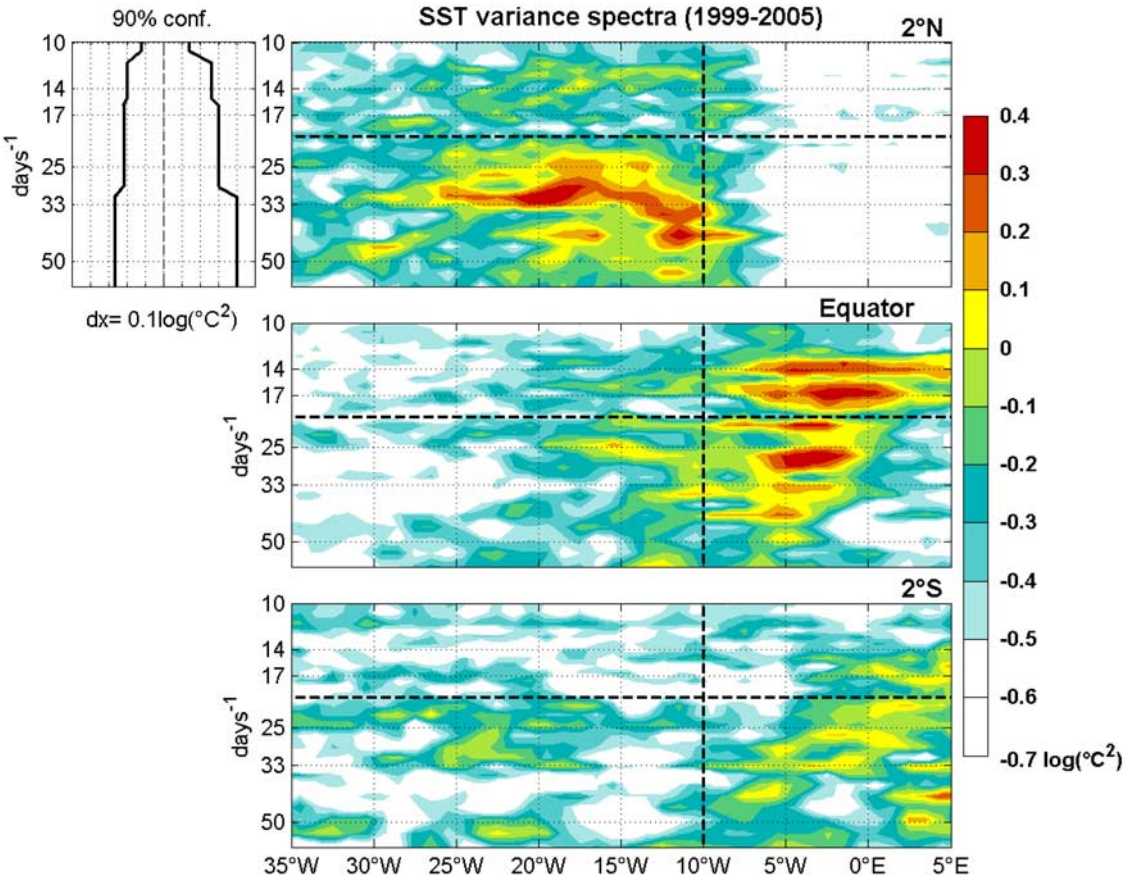

Figure 6. Same as Figure 5 for SST along (top) 2°N, (middle) equator, and (bottom) 2°S with respect to frequency (in logarithmic scale). Contour interval is 0.1 log(°C^2). The 90% confidence interval is 0.65 log(°C^2) for 30–60 days, 0.5 log(°C^2) for 15–30 days, and 0.45 log(°C^2) for 10–15 days. Variances are normalized by the zonally averaged variance for the corresponding 10- to 50-day anomalies, namely, 0.2°C^2 at 5°N and 0°N and 0.1°C^2 at 5°N.

southern hemisphere along 2°S (between 35°W and 10°W) and near 5°S (between 35°W and 18°W). Note that the lowest standard deviations of SLA between 10°N and 10°S are found to be 0.9 (confidence interval of 0.8–1.1 cm) in a large region east of 10°W, indicating that the southern maximum is significant with respect to the background variability in the Tropical Atlantic Ocean. High variability can also be observed along the African coast, but it is not clear whether this signal is related to coastally trapped waves [*Picaut*, 1983] or an artifact of near coastal altimeter measurements.

[21] SST standard deviation shows a different geographical pattern (Figure 2b). The highest standard deviation (~0.6°C) is located along a line that goes from 1°S, 5°E to 2°N, 20°W. This line matches the northern front of the seasonal cold tongue (that takes place every summer in the eastern part of the equatorial Atlantic Ocean). The properties of the SST intraseasonal variability west of 10°W have already been found to be associated with TIWs [*Caltabiano et al.*, 2005], but the origin of SST intraseasonal anomalies in the Gulf of Guinea still needs to be clarified.

3.2. Propagation Properties

[22] Longitude-Time diagrams of SLA and SST anomalies in 2002 illustrate the main characteristics of intraseasonal variability along the latitudes of highest variability (Figure 3). A succession of negative/positive intraseasonal SLA anomalies are observed from May to September along 5°N west of 10°W (Figure 3a). These anomalies propagate westward and their amplitude can reach 9 cm. Their wavelength is close to 1000 km and their phase speed was estimated using Radon transform [*Challenor et al.*, 2001] to be 42 cm/s, in agreement with previous observations [*Weisberg and Weingartner*, 1988].

[23] South of the equator (5°S) anomalies of weaker amplitude can also be identified in SLA west of 10°W during the same period of the year (Figure 3b). Their amplitude does not exceed 6 cm, with wavelengths (~1000 km) comparable to the ones observed along 5°N and slightly slower zonal propagation velocities (31 cm/s).

[24] The longitudinal and temporal distribution of SST anomalies is far more complex (Figures 3c–3e). West of 10°W westward-propagating anomalies are dominant. Their amplitude is maximum along 2°N (>1.5°C) propagating at 40 cm/s during boreal summer, at the same season as SLA along 5°N. They can also be seen along the equator and 2°S with a phase propagation speed of 39 cm/s. This signal has comparable wavelength and zonal phase speed to SLA anomalies and is the SST signature of the TIWs [*Chelton et al.*, 2000; *Caltabiano et al.*, 2005].

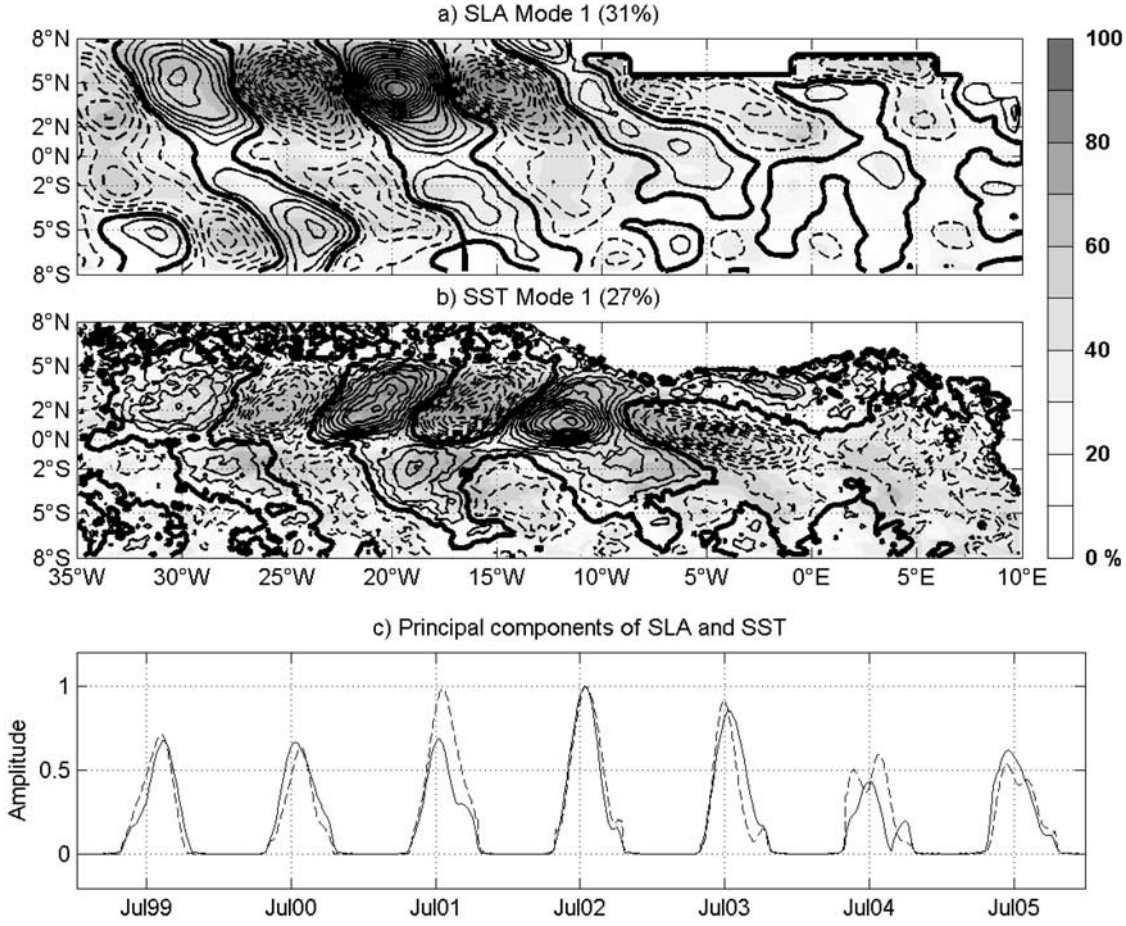

Figure 7. First CEOF mode of 25- to 50-day filtered SLA and SST for the whole period of 1999–2005: real part of the spatial modes in (a) SLA and (b) SST and the temporal modulation amplitude (c, SLA: solid line; SST: dashed line). Contour intervals are 0.5 cm for SLA and 0.1°C for SST (negative values are in dashed line). The local explained variance (in %) is superimposed (see color map). Data before 1 May and after 30 September of year of each year have been set to zero in the computation.

[25] East of 10°W, SST anomalies with comparable magnitude are observed in boreal summer. However, unlike the TIWs, they are intensified along the equator (Figure 3d), though still detectable at 2°S, and do not show any clear zonal propagation. They have no signature in SLA (not shown).

[26] Longitude-Time diagrams during the TIWs season and for the whole period 1999–2005 are shown in Figure 4 for the SLA at 5°N and 5°S. Both, northern and southern anomalies are present every year, in the same season, though always weaker in the southern hemisphere. Mean phase velocities have been estimated to be 40 ± 3 cm/s in the Northern Hemisphere and 28 ± 5 cm/s in the southern hemisphere, indicating that southern anomalies propagate slightly more slowly than their northern counterparts. Intense interannual variability can be observed, with the strongest amplitudes (>8 cm) in 2002 and 2003 and the weakest (<4 cm) in 2004. This differs from the interannual variability of TIW activity deduced from SST alone [*Wu and Bowman*, 2007], where for the same years strongest TIW activity was found in 2001 and 2004 (their Figure 3b).

3.3. Dominant Periods of Intraseasonal Variability

[27] The longitudinal structure of dominant periods of SLA/SST intraseasonal variability can be inferred from the longitude-frequency diagrams of variance spectra (Figures 5 and 6).

[28] The dominant variances in SLA are found in the range 25–60 days along the three latitudes of highest variability (5°N, 2°S, 5°S) (Figure 5). The strongest variances are located at 5°N (Figure 5a). Between 30°W and 10°W, maximum variances are found in a broad range of periods extending from 25 to 50 days, exceeding 15 cm^2 for periods near 32 days between 25°W and 15°W and 40 days between 20°W and 35°W. This range of periods corresponds to TIWs as described for instance by *Weisberg and Weingartner* [1988]. In contrast, west of 30°W, the variability is confined to periods between 40 and 60 days and no more variability is observed at periods near 30 days. This corresponds to meanders of the NECC [*Garzoli*, 1992], that originate from the barotropic instability of the NECC in the western part of the basin [*Jochum and Malanotte-Rizzoli*, 2003]. In the south (2°S and 5°S), variances are maximum west of 10°W and present a

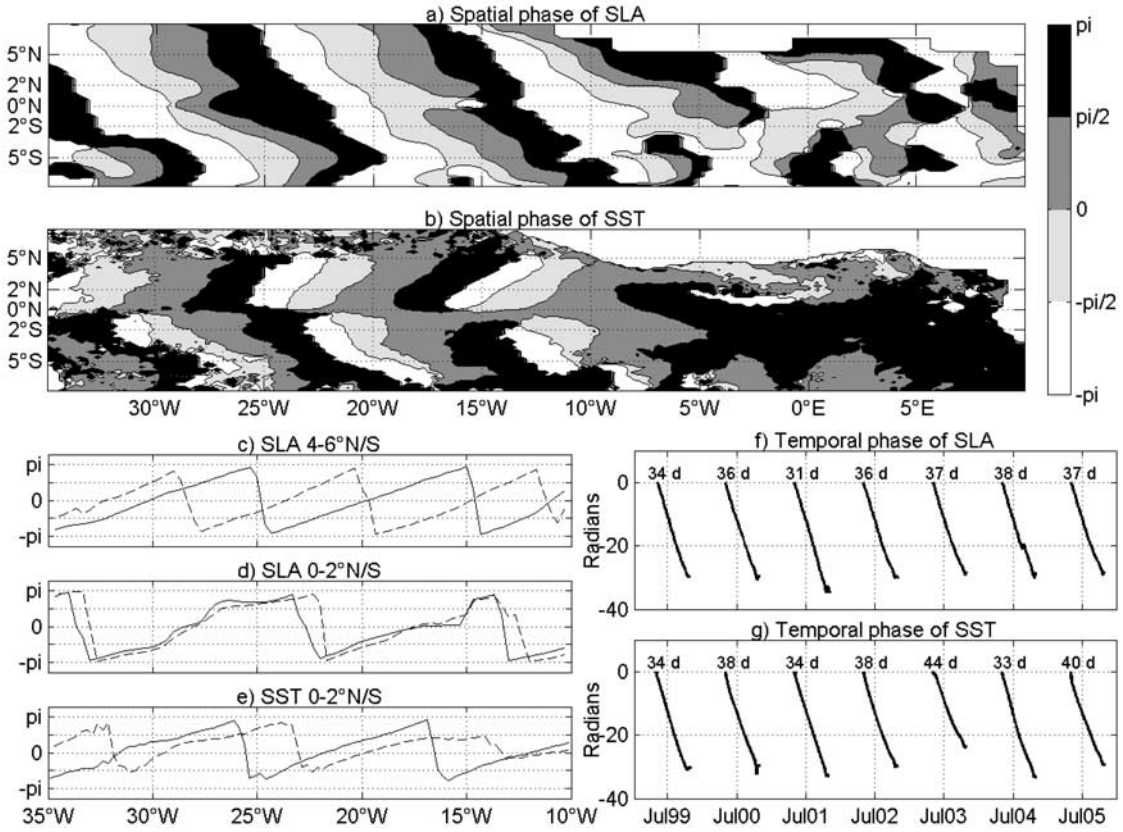

Figure 8. First CEOF mode of 25- to 50-day filtered SLA and SST for the whole period of 1999–2005: horizontal distribution of phase in (a) SLA and (b) SST. Mean phase (c) between 4° and 6°N/S and (d) between the equator and 2°N/S for the SLA and (e) for the SST between the equator and 2°N/S (northern mean phase: solid line; southern mean phase: dashed line). Temporal phase is calculated from the principal components of (f) SLA and (g) SST. The negative slope of the temporal phase indicates westward propagation. The corresponding periods (in days), estimated every year from linear fitting of the temporal phase, are indicated in the figure (errors on the linear fitting are lower than 2 days for the SLA and 1 day for the SST). Data before 1 May and after 30 September of each year have been set to zero in the computation.

similar longitudinal distribution in the range 25–60 days, but their amplitude does not exceed 5 cm^2. An interesting feature is that maximum variance at 2°S is found for periods about 32 days near 20°W, whereas the dominant variability over 30°W–15°W is rather centered around 40 days. The two distinct peaks of variability that were evidenced in the center of the basin along 5°N are thus retrieved south of the equator, but weaker and at two different latitudes.

[29] The variance spectrum of SST (Figure 6) reveals a more complex structure in frequency than observed for SLA. North of the equator (2°N) the variability is confined to the region west of 10°W (Figure 6a). The dominant periods are observed in a broad frequency band between 25 and 50 days, in concordance with SLA, extending from 30°W to 10°W. Two local maximum are observed in this frequency range: one exceeding the 0.4°C^2 is centered around 32 days and correspond to the SST signature of TIWs, as discussed by *Caltabiano et al.* [2005]; the second one of 0.3°C^2 is particularly visible between 20°W and 8°W centered at 40 days.

[30] The longitude-frequency SST distribution along the equator shows striking differences with respect to SST at 2°N and to SLA at 5°N. A remarkable new feature at this latitude is the presence of an intense variability at periods between 10 and 20 days. This variability is confined to the Gulf of Guinea and has no signature in SLA or SST north of the equator, and corresponds to the nonpropagating equatorially trapped signal that was observed in longitude-time SST diagram (Figure 3). Moreover, anomalies in the TIW frequency range (25–50 days) are also observed along the equator. However, unlike 2°N where they were observed only west of 10°W, these anomalies are now maximum east of 10°W (0.5°C^2). Both 10- to 20-day and 25- to 50-day signals along the equator have comparable magnitudes, of the same order as the one we have identified before along 2°N.

[31] In the southern hemisphere (at 2°S, Figure 6c), unlike the signal at 2°N, the dominant signals are located in the Gulf of Guinea, where the periods corresponds to those observed at the equator, but with weaker amplitude (around 0.1°C^2). West of 10°W, there is a patch of maxi-

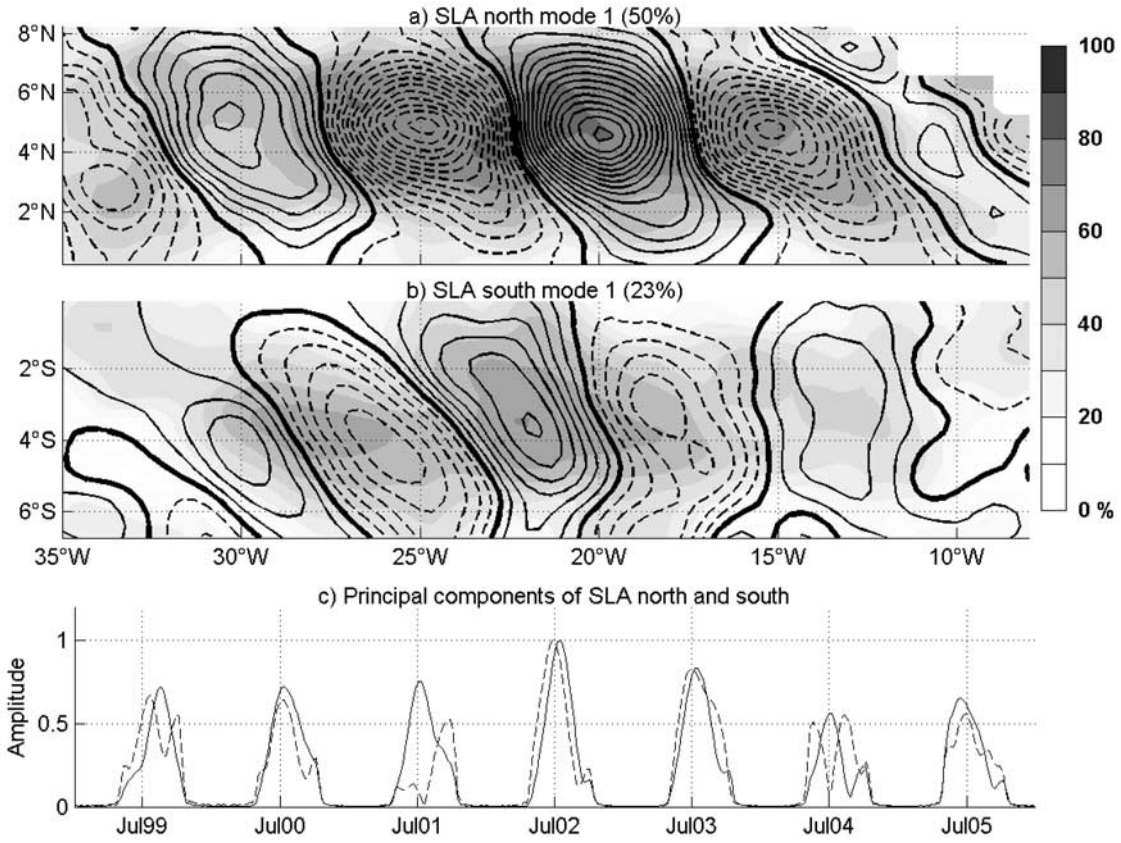

Figure 9. Same as Figure 7 for the SLA, but the CEOF analysis is performed separately for the Northern and Southern Hemispheres: (a) spatial mode of the northern CEOF, (b) spatial mode of the southern CEOF, and (c) temporal modulation of the amplitude (northern CEOF is in solid line and southern CEOF is in dashed line).

mum variability (lower than $0.1°C^2$) between 30°W and 15°W and with periods between 25 and 35 days. This signal has the same periods and longitudinal distribution as the SLA signal along 2°S.

[32] In the following sections we will address separately and in more details the respective spatial structure and interannual variability of the TIWs, and of the equatorially trapped SST signal in the Guinea Gulf (referred hereafter to as the 15-day variability). To do so, we have decomposed SST and SLA 10- to 50-day signal into 25- to 50-day and 10- to 20-day anomalies. Since this study focuses on the properties of TIWs in the center of the basin, a 25- to 50-day band-pass filter has been chosen, which better isolates TIWs east of 30°W but excludes the variability that has longer periods west of 30°W.

4. Properties of the TIWs

[33] CEOF analysis has been computed separately for 25- to 50-day anomalies in SLA and SST to describe the dominant spatial pattern and interannual modulation of the TIWs for the whole period 1999–2005 (Figure 7). Since the TIWs season occurs between May to September (Figures 3 and 4), data are set to zero before 1 May and after 30 September of each year in the computation to better isolate the TIW signature. Similar CEOF decompositions were performed taking into account the yearlong signal, or combining SLA and SST data (not shown). The spatial modes are comparable in all cases, but computing CEOF separately and extracting the TIW season allows us first to enhance the explained variance and then to compare the temporal variability of the two signals.

4.1. Mean Cross-Equatorial Structure

[34] Figure 7 presents the real part of the empirical function for the first CEOF mode of SLA and SST. The spatial structure of the first mode in SLA (Figure 7a) shows zonal tracks of successive positive/negative anomalies that reproduces the main characteristics of the TIWs. It represents 31% of the total variance, but more than 50% of the explained local variance in the regions of highest variability. As expected, the strongest amplitudes (~7 cm) are found in the Northern Hemisphere, west of 10°W. They are centered at 5°N extending from 2°N to 7°N with a typical zonal wavelength of 1000 km. The second most important amplitudes (~2 cm) are located along 5°S, with a wavelength comparable to the one observed at 5°N, but in a less organized pattern. The corresponding spatial phase diagrams (Figure 8a) shows that phases vary with latitude. However a close examination of phases along 5°N and 5°S (Figure 8c) shows an out-of-phase relationship, suggesting that anomalies along 5°N and 5°S propagate together as a single feature. This spatial mode has periods around 35 days and propagates westward (Figure 8f).

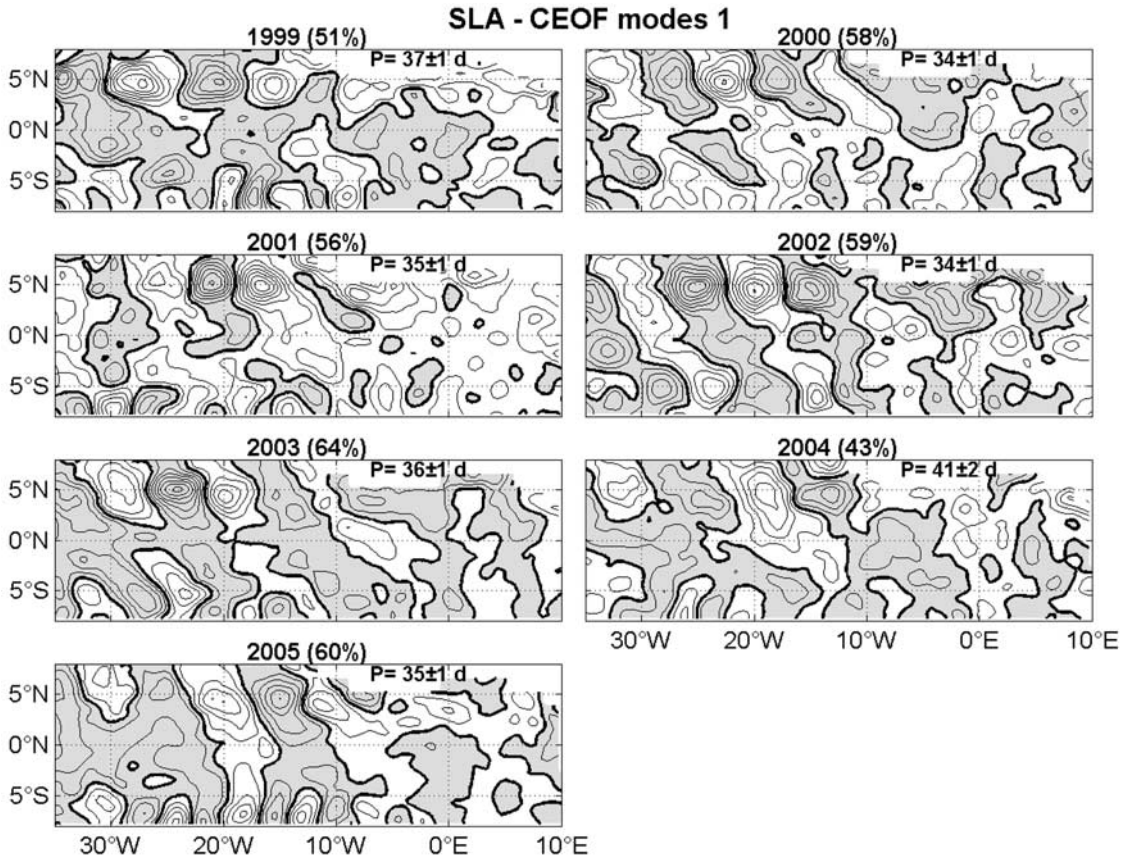

Figure 10. Real part of the first CEOF mode of 25- to 50-day filtered SLA for every year from 1999 to 2005. Contour interval is 1 cm, and negative values are in gray. The percentages of total variance explained by each mode are indicated in titles. The periods and corresponding errors estimated every year from linear fitting of the temporal phase are indicated in each. Data before 1 May and after 30 September of each year have been set to zero in the computation.

[35] The other latitude of maximum variability (2°S) is also captured by the first mode of SLA (Figure 7a). At this latitude, anomalies greater than 1 cm are present from 35°W to 10°W. The phase diagram (Figures 8a and 8d) shows that the anomalies between 2°S and 2°N are not out of phase, but are predominantly in phase. Moreover the phase lines in Figure 8a are parallel at all latitudes, meaning that 5°N/5°S and 2°S anomalies propagate at similar speeds, even though the dynamical relationship between these two signals needs to be clarified.

[36] An equivalent CEOF decomposition of SLA anomalies has been performed separately north and south of the equator, representing 50% and 23% of the variability respectively. The spatial structures on both sides of the equator (Figures 9a and 9b) are similar to the ones obtained in Figure 7a. This indicates that the cross-equatorial structure of TIW evidenced in Figure 7 is the dominant variability in boreal summer both north and south of the equator. Besides, the year-to-year variability of the principal components for the northern and southern CEOF shows a close correspondence, except in 2001. The amplitudes of the northern and southern spatial structures are thus mostly linked together, providing further evidence that they are the northern and southern signatures of the same variability.

[37] The first CEOF mode in SST represents 27% of the total variance and more than 50% of the explained local variance near the equator (Figure 7b). SST anomalies west of 10°W shows alternate positive/negative signs, with similar wavelengths and periods than the first mode in SLA (Figure 8g). The amplitude of the signal north of the equator is stronger than the signal in the southern hemisphere. Note the elongated shape of the northern anomalies that has already been evidenced by *Caltabiano et al.* [2005]. Figures 8b and 8e show that anomalies at 2°N and 2°S are mainly in quadrature west of 10°W.

[38] Unlike the spatial mode of SLA, significant anomalies also show up in the first CEOF SST mode east of 10°W, in the Gulf of Guinea. These anomalies, which were already described by *Bunge et al.* [2007], are centered at the equator between 10°W and 0°E. The corresponding phase diagram (Figure 8b) shows no clear zonal propagation for these anomalies. This explains why these anomalies were not identified in *Caltabiano et al.* [2005] in which a westward-only filter was applied to SST data. The fact that this equatorial structure is part of the first CEOF mode suggests that it is an important pattern of the intraseasonal variability even if it has no signature in SLA.

[39] The principal components of the first modes in SLA and SST reproduces some interannual variability

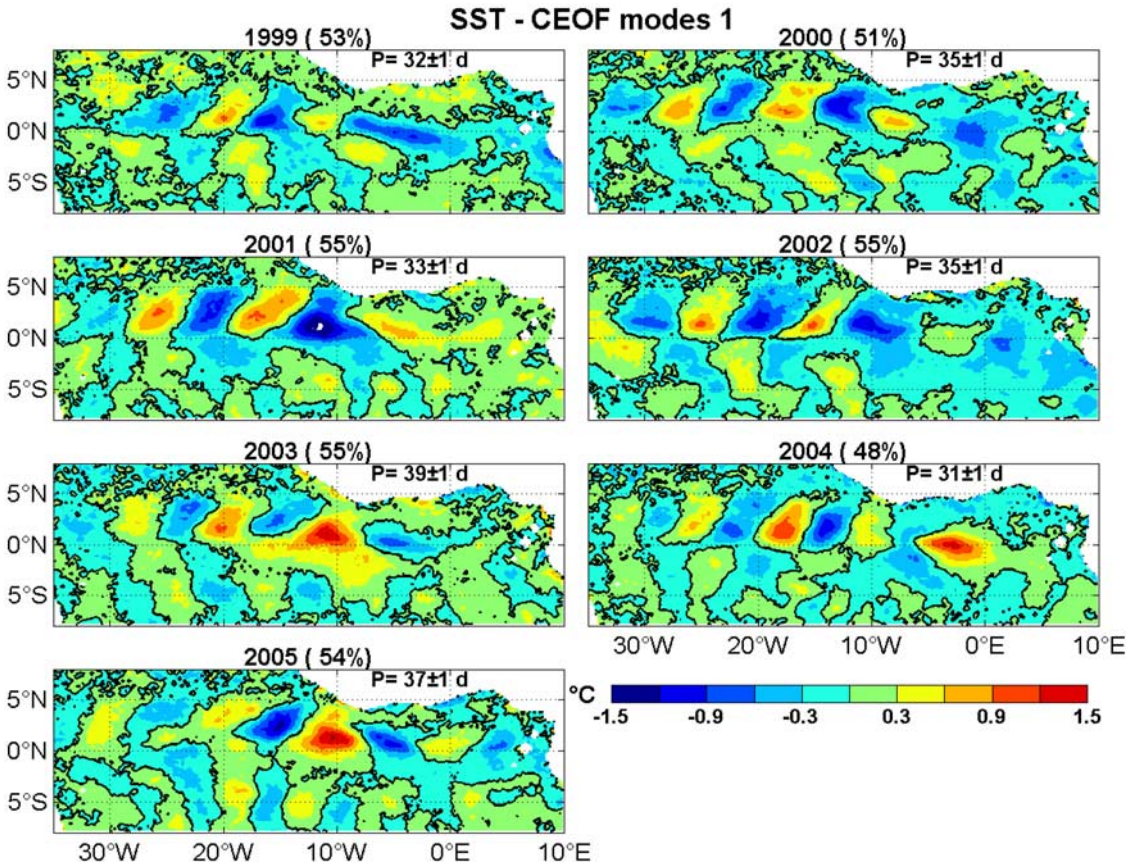

Figure 11. Same as Figure 8 for the SST. Contour interval is 0.3°C, and solid line indicates the 0°C anomalies.

(Figure 7c), the TIW activity being more intense for both data sets in 2002 and 2003 and weaker in 2004 and 2005. If the amplitudes of SLA and SST anomalies compare well most of the years, it is not the case in 2001 where SST amplitude is one of the more intense of the period 1999–2005 whereas the amplitude in SLA is moderate.

4.2. Interannual Modulation

[40] In the previous section, it has been demonstrated that the mean surface signature of TIWs over 1999–2005 was not limited to the Northern Hemisphere, but project also in the southern hemisphere, suggesting the presence of cross-equatorial structures in SST and SLA that propagate westward together west of 10°W. This contrasts with *Steger and Carton* [1991] who did not evidence a clear phase relationship between the TIWs north and south of the equator from the analysis of SST snapshots over the period 1984–1990. However it is not clear from first CEOF modes alone that such cross-equatorial structures are permanent patterns of TIW variability year after year. Moreover the first CEOF modes in SLA and SST only represent 30% of the total variance and thus do not capture the full surface signature of TIWs. In order to determine the year-to-year variability of the TIWs cross-equatorial structure itself, CEOF analyses for SLA and SST were repeated for each individual year.

[41] The first CEOF modes of the SLA data for every year (Figure 10) represent more than 50% of the total variance. As in the first CEOF modes for the whole period 1999–2005, positive/negative anomalies can be clearly observed every year along 5°N with ~1000-km wavelength and maxima amplitude ranging from 4 cm in 2004 to >8 cm in 2002. In the southern hemisphere, the intraseasonal variability is more complex and is seen to vary from one year to another. Intraseasonal anomalies are observed between 3°S and 5°S in 2000, 2002 and 2003, and in a lesser extent in 1999, when the TIW activity in the Northern Hemisphere is the strongest. As in the 1999–2005 CEOF mode, these anomalies are out of phase (not shown) and weaker when compared to their 5°N counterparts. In contrast, in 2001, 2004 and 2005 years where structures between 2°S and 5°S were weaker, variability in the southern hemisphere is mainly dominated by 500-km wavelength mesoscale structures located more southward, near 7°S, with a maximum amplitude of 4 cm. This variability is seen to be present every year, though with different amplitudes from one year to another. Finally, between the equator and 3°S, the intraseasonal variability is more variable interannually but can be distinguished for instance in 1999 or 2002. This signal does not dominate the southern variability during any year and its amplitude does not exceed 2 cm.

[42] The first CEOF modes in SST represent more than the 48% of the total variance every year (Figure 11). The TIWs spatial structure closely resembles the first CEOF mode in SST that was computed for the whole period

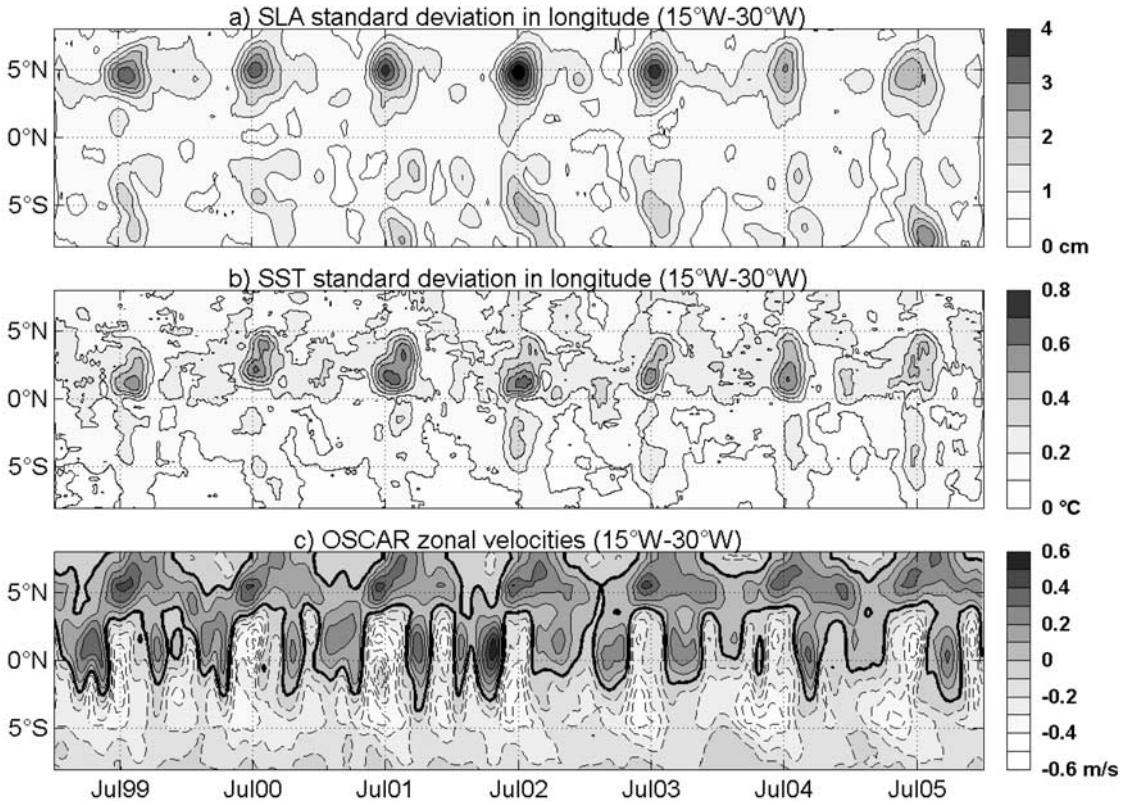

Figure 12. Time-Latitude plots of the standard deviation of 25- to 50-day filtered (a) SLA and (b) SST and of the low-pass-filtered (>50 days) OSCAR zonal velocities. (c) The fields are zonally averaged over the longitudes 30°W–15°W. Units are centimeters for SLA, degrees centigrade for SST, and meters per second for zonal velocities.

1999–2005, and is similar throughout the years in the vicinity of the equator, in contrast with SLA where variability in the southern hemisphere were highly variable from one year to another. The TIWs signature in SST is dominated by a double-hemisphere pattern with two latitudes of maximum variability near 2°N and 2°S where structures of 1000-km wavelength are found to be in quadrature (not shown), as in the mean CEOF mode for 1999–2005. The highest amplitudes at 2°N are observed in 2001 and 2004, in agreement with *Wu and Bowman* [2007]. Note that the strong SST anomalies in 2004 coincide with moderate anomalies in SLA, suggesting that the large amplitude of these anomalies is not due to TIW dynamics, but rather to a more intense SST front north of the equator in response to a colder than usual cold tongue in this particular year [*Wu and Bowman*, 2007]. In addition, distinct maxima of variability are found between 3–4°S and 8°S with shorter wavelengths (~500 km) and correspond to anomalies observed in SLA at the same latitude. Finally, the nonpropagating variability east of 10°W is present every year.

[43] These results emphasize that the mean spatial structures in SLA and SST computed for 1999–2005 (Figures 7 and 8) provide a robust description of the cross-equatorial structure of the TIWs, in particular the out-of-phase relationship between SLA anomalies along 5°N and 5°S and the quadrature between SST anomalies along 2°N and 2°S. However, whereas the TIWs structures in the Northern Hemisphere are shown to be persistent throughout the years, the variability in the southern hemisphere proves to be more variable from one year to another, especially between the equator and 3°S, with an additional variability more southward between 5°S and 8°S.

4.3. Seasonal Evolution

[44] Figure 12 shows the time-latitude distribution of the zonally averaged standard deviation of 25- to 50-day anomalies for both data sets between 30°W and 15°W. Unlike SLA, which highest 25- to 50-day variability is centered every year on boreal summer at 5°N (Figure 12a), the latitude of maximum variability in SST is indeed seen to vary between 1°N and 3°N from one year to another, mainly in response to the year-to-year meridional migration of the SST front north of the boreal summer cold tongue. In the southern hemisphere, Figure 12a reproduces the three latitudes of maximum variability (2°S, 5°S and 7°S) that were described in the previous section. Interestingly, the variability in SLA along 2°S and 7°S is mostly observed to occur after the peak of the TIWs season, suggesting that the southern signature of TIWs, along 5°S, is not the only source of variability south of the equator. In contrast, the intraseasonal variability in SST north and south of the equator is seen to be more simultaneous.

[45] TIWs are triggered by oceanic instabilities of the seasonally varying currents and hydrological structure. To assess the role of surface seasonal zonal currents shear for

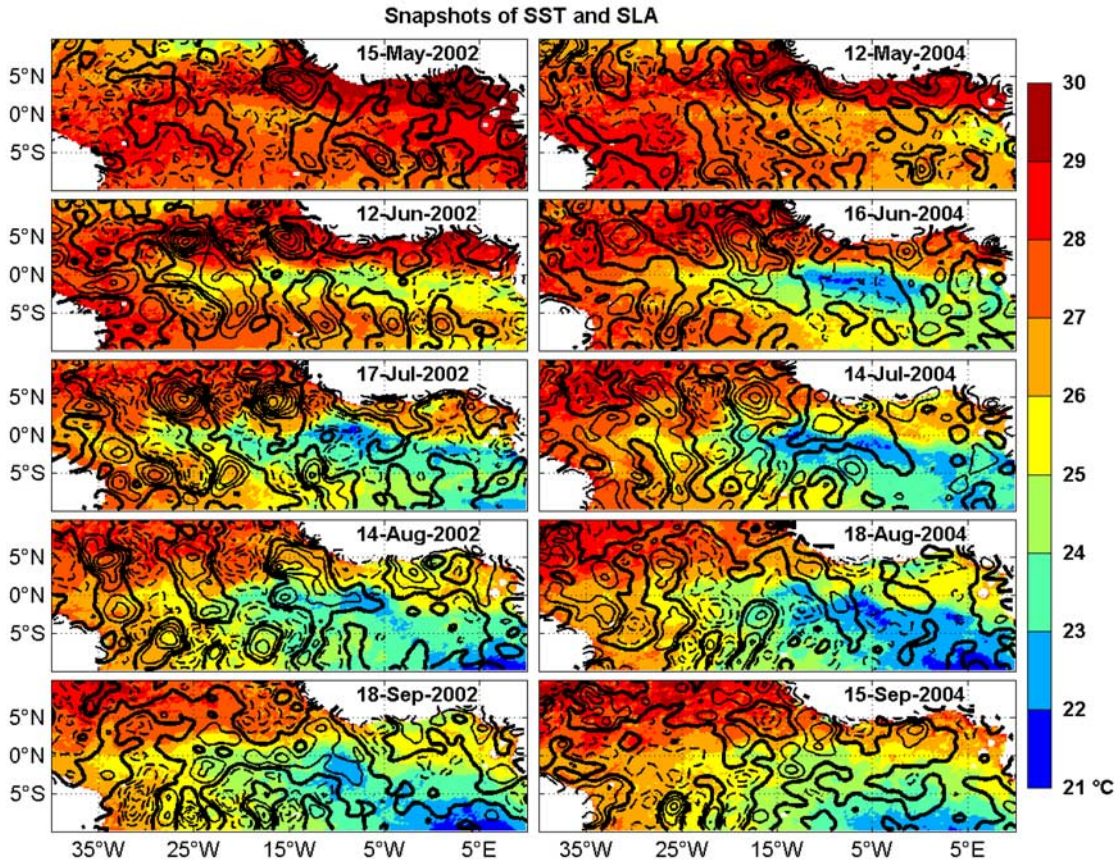

Figure 13. Snapshots of the horizontal distribution of SST (colored) and 25- to 50-day filtered SLA (contours) each month from (top) mid-May to (bottom) mid-September for (left column) 2002 and (right column) 2004. Contour interval for SLA anomalies is 1 cm (negative values are in dashed line).

the generation of 25–50 days SLA anomalies, we compare the time-latitude distributions of the SLA anomalies standard deviation and of the low-pass (>50 days) OSCAR zonal currents (where TIWs variability has been filtered out), both zonally averaged over 30°W–15°W (Figures 12a and 12c). SLA variability is found to be maximum in boreal summer of every year, when eastward (westward) velocities are the strongest at 5°N (2°N) and the meridional shear between the NECC and the SEC is positive and maximum giving birth to barotropic instabilities [e.g., *Philander*, 1976, 1978]. The correlation between the intensity of the NECC and the TIW amplitude along 5°N is found to be 0.71 ± 0.04. A description of the NECC seasonal variability can be found in *Garzoli* [1992]. Note that there is no such meridional shear in the southern hemisphere, suggesting that the southern component of TIWs is not created locally through the instability of the surface currents, but rather related to the either variability north of the equator or below the surface. Besides no clear correspondence was identified between the interannual variability in SLA anomalies and the intensity of OSCAR zonal currents in boreal summer, which does not allow us to conclude about the origin of TIWs interannual variability. The vertical and horizontal shear between the EUC and the SEC beneath the surface is another source of instability [e.g., *Qiao and Weisberg*, 1998] that may play role in the TIW year-to-year variability, but this cannot be observed from satellite data.

[46] To describe in more details the seasonal evolution of TIWs anomalies in SLA and SST, Figure 13 presents snapshots of the horizontal distribution of SST and of 25- to 50-day anomalies in SLA for two specific years (2002 and 2004). TIWs variability in SST has already been described for 2002 by *Bunge et al.* [2007], but snapshots of SLA anomalies provide additional information about the temporal evolution of the spatial structure of this variability. In 2002, the TIWs season began in mid-May, with the appearance of organized anomalies in SLA along 5°N (reaching 7 cm in amplitude in June at 20°W). In mid-June, anomalies in SLA are intensified along 5°N, with weaker out-of-phase counterparts along 5°S, that both persist in July. In terms of SST, large meanders of the SST front were observed in June simultaneously to SLA anomalies from 2°S to 2°N. During July, anticyclonic filaments of cold waters were seen to form progressively poleward of 2 degrees in latitude in each hemisphere at the location of the positive zonal gradient of SLA anomalies, i.e., where anomalous meridional geostrophic velocities were poleward. Conversely, warm waters penetrated equatorward at the longitudes of negative zonal gradient of SLA anomalies, i.e., where anomalous meridional geostrophic velocities were equatorward. In mid-August, filaments of SST were still present north of the equator and west of 20°W, but were no longer visible east of 20°W or in the southern hemisphere where the southward extension of the cold tongue

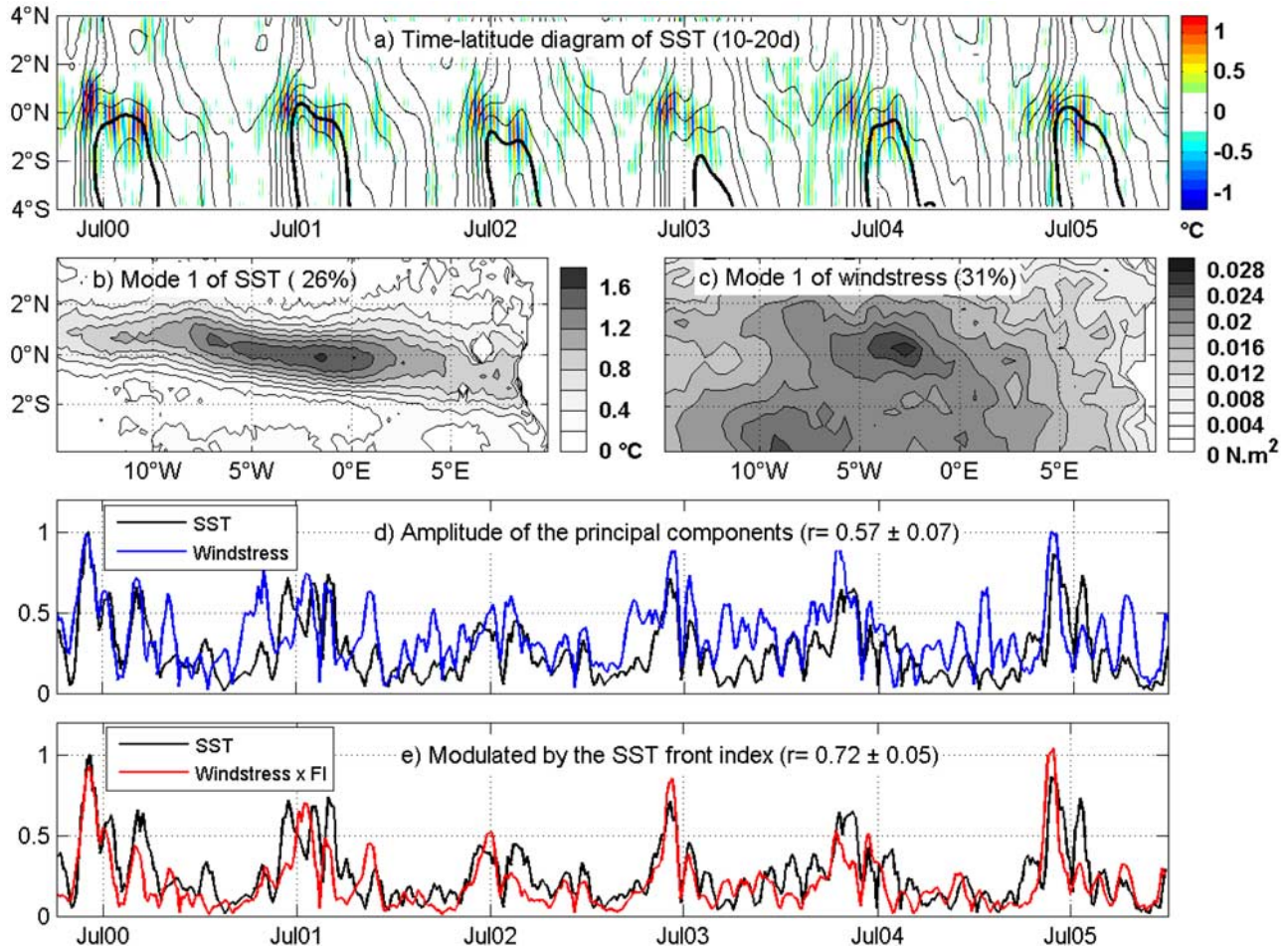

Figure 14. Spatial and temporal distribution of 10- to 20-day filtered SST and QuickSCAT meridional wind stress. (a) Time-Latitude plot of 10- to 20-day SST anomalies zonally averaged over 5°W–0°E. Contours are the SST low-pass-filtered (periods >50 days); contour interval is 1°C; 24°C isotherm is in thick line. First EOF modes of the 10- to 20-day anomalies in (b) SST and (c) meridional wind stress; contour interval is 0.2°C for SST and 2.5 10^{-3} N m^2 for wind stress. (d) Amplitude of the corresponding principal components in SST (solid line) and meridional wind stress (blue line). (e) Same as Figure 14d, but the meridional wind stress amplitude is multiplied by the SST front index (red line) as defined in the text.

suppressed the background SST gradient that is required to observe TIWs. Meanwhile, the dominant out-of-phase TIWs began to disorganize, especially along 5°S, and were progressively replaced by successive positive/negative anomalies along 6°S, which become stronger in September and do not have counterpart in the Northern Hemisphere. At 6°S, the SLA anomalies had amplitude of the order of 3 cm, typical wavelength of 500 km and westward phase speeds of about 17 cm/s. *Bunge et al.* [2007] showed the existence of this intraseasonal variability, but with SST observations alone. It must be noted that SLA anomalies of amplitudes close to 2 cm were observed along 2°S in 2002 from mid-May to mid-September, appearing at the same time as TIWs but becoming stronger in mid-August and lasting beyond the TIWs season. It is not clear whether the various forms of intraseasonal variability contributed to the progressive widening of the equatorial cold tongue.

[47] The patterns of 25- to 50-day variability in 2004 were quite different. While SLA coherent structures were also observed with wavelengths of 1000 km along 5°N from May to July, they were weaker than in 2002 and had no clear counterpart in the southern hemisphere, thus departing from the dominant TIWs captured by the 1999–2005 CEOF decomposition. Nevertheless, larger meanders and filaments in SST were seen during mid-July of that year, extending as far as 5°N, but the distance between two successive filaments proved to be less (about 700 km) than in 2002 (about 1000 km). SLA anomalies along 5°N thus cannot fully explain the characteristics of the intraseasonal variability in SST more equatorward and other mechanisms may be at play to create/maintain these filaments in 2004. However, the intraseasonal variability in SLA along 2°S had the same characteristics in 2002 and 2004, and the 500-km wavelength SLA anomalies were once again present from August till September.

5. Biweekly Signal

[48] As seen in the longitude-time diagram of SST anomalies (Figure 3), another strong intraseasonal variability was present in the Gulf of Guinea, with periods between

10 and 20 days and no clear zonal propagation. This signal that is equatorially trapped and has no signature in SLA was already observed in the Equatorial Atlantic both in current meter data and in SST [*Bunge et al.*, 2006]. This variability has been associated with mixed Rossby-gravity waves that have maximum meridional velocities right at the equator and are thought to be mainly forced by the intraseasonal anomalies in meridional wind stress [*Houghton and Colin*, 1987], even though tropical instabilities are likely to play also a role in their generation at depth [*Düing et al.*, 1975].

[49] To identify the geographical distribution and temporal evolution of this variability, an EOF analysis on the 15-day SST anomalies was performed from 2000 to 2005 in the region where this variability was observed, i.e., [15°W–10°E] × [4°S–4°N]. Figures 14b and 14d show respectively the spatial mode (that represents 26% of the total variance) and the amplitude of the principal component of the first EOF mode. The amplitude was computed as the maximum value over successive 5-day windows. The spatial SST variability mode is confined to a narrow equatorial region, and amplitudes are maximum along a tilted line that corresponds to the northern front of the seasonal cold tongue (Figure 14b). There is a clear seasonal variability with maximum amplitude in boreal summer (Figure 14d). This maximum SST variability coincides with periods of the year when the SST front near the equator is most intense (Figure 14a).

[50] The first EOF mode of 10- to 20-day meridional wind stress was computed to assess the role of the local intraseasonal wind stress anomalies for the generation of the 15-day SST variability (Figure 14b). The EOF analysis was calculated within the same region, [15°W–10°E] × [4°S–4°N], as for SST. This mode, which accounts for 31% of the total variance, shows that a significant variability in meridional wind stress is present in the same band of frequencies. The spatial structure of this mode shows that the 15-day anomalies in wind stress are located over a region, extending from 4°S to 2°N and from 15°W to 5°E that is far larger than the region where 15-day anomalies in SST are observed. Note however the presence of a local maximum along the equator, near 3°W, at the location of the maximum in SST anomalies, which may be the local signature of a possible retroaction of the SST anomalies over the atmosphere just above. The amplitude of the corresponding principal component (solid line in Figure 14d) shows that, unlike the first EOF mode in SST, the 15-day variability in meridional wind stress is present throughout the year and is not seasonally locked to boreal summer, though the maximum amplitudes are mostly found in June. However there is a close peak-to-peak correspondence between the two time series in Figure 14d, with a correlation of 0.57 ± 0.07.

[51] To study how the magnitude of the SST front seasonally modulates the amplitude of the 15-day signal in SST, a SST front index (FI) was computed from the time series of low-pass-filtered SST data (periods greater than 50 days) to represent the intensity of the northern front of the boreal summer cold tongue. This front index is defined as $(T_N - T_S)/L$, where T_N and T_S are the spatially averaged low-pass-filtered SST over respectively [10°W–0°E] × [3°N–4°N] and [10°W–0°E] × [1°S–0°N], and L is 4° in latitude. The amplitude of the first EOF principal component of the wind stress (blue line in Figure 14d) is then multiplied by the FI (red line in Figure 14e). The time evolutions of the first EOF modes in FI-modulated wind stress and in SST are now quite similar, with a correlation coefficient increasing to 0.72 ± 0.05. This demonstrates that the 15-day signal at the surface of the ocean is forced by intraseasonal anomalies in meridional wind stress at the same periods, but that its signature in SST is strongly influenced by the presence and intensity of the cold tongue front.

6. Summary and Conclusion

[52] The intraseasonal (10–50 day) variability at the surface of the tropical Atlantic has been analyzed from the comparison of multiyear satellite observations of SLA and SST over the period 1999–2005. This variability was shown to be the most intense in boreal summer for both data sets. This paper evidences the existence of two principal signals that dominate the variability in two distinct regions, west of 10°W and east of 10°W. The first one has periods between 25 and 50 days and was observed at off-equatorial latitudes in both SLA and SST. It corresponds to the surface signature of TIWs. The second dominant signal was observed within the Gulf of Guinea with periods between 10 and 20 days, and only had a signature in SST.

[53] An important result of this study is that the TIWs have a signature in SST and SLA both north and south of the equator with the same range of wavelengths (∼1000 km), phase velocities (25–45 cm/s) and periods (30–45 days), indicating that TIWs are essentially a westward-propagating cross-equatorial wave pattern. In SLA, the strongest anomalies associated with TIWs are found along 5°N and 5°S, though they are twice weaker in the southern hemisphere than north of the equator. A similar cross-equatorial structure in SLA has been evidenced in the Pacific Ocean by *Lyman et al.* [2005] and explained as a first meridional mode Rossby wave, whose meridional structure is modified by the background zonal currents [see also *Proehl*, 1998], leading to larger amplitudes at 5°N. The evidence of comparable cross-equatorial SLA variabilities in the Pacific and in the Atlantic indicates that Rossby waves must be the main contributor for TIW dynamics in the Atlantic too. However, contrary to the Pacific Ocean where SLA anomalies north and south of the equator are found to be mainly in phase [*Lyman et al.*, 2005], we have evidenced the presence of an out-of-phase cross-equatorial structure in the Atlantic in the present study. This suggests that a second meridional mode of equatorial Rossby waves is likely to participate to the TIWs variability in the equatorial Atlantic Ocean, even though more thorough studies would be needed to determine the precise cross-equatorial structure of equatorial waves in the presence of mean zonal currents.

[54] In SST, the dominant pattern for TIWs has maximum amplitudes at 2°N and 2°S west of 10°W, with amplitudes twice greater in the Northern Hemisphere as in SLA. This spatial mode has been shown to be a robust pattern that is present every year. Unlike SLA, SST anomalies associated with TIWs are observed to be mostly in quadrature north and south of the equator. Such discrepancies in the phase relationships between northern and southern anomalies in SLA and SST shows that the dynamics of the dominant

5°N/5°S pattern in SLA cannot fully explain the SST signature of TIWs west of 10°W.

[55] Finally, the TIW signatures in SLA and SST are shown to experience a comparable year-to-year variability in their magnitude, suggesting that the interannual variability in TIW signature in SST is a good indicator of the variability of the TIWs dynamics itself. However, in 2001, the amplitude of the TIWs was seen to be higher in SST than in SLA. This could be related to the presence of a stronger cold tongue in 2001, as evidenced by *Wu and Bowman* [2007], that amplifies the intensity of the SST front which is required for the TIWs to be observed.

[56] Additional signals of 25- to 50-day variability have been evidenced in this study. First a 25- to 50-day variability has been found in SST within the Gulf of Guinea, but, unlike the variability west of 10°W, it does not propagate westward and is centered at the equator. Besides, intraseasonal variabilities along 7°S, and between the equator and 3°S, have been shown to contribute also to the year-to-year modulation of the TIW signature in SLA. A numerical study by *von Schuckmann et al.* [2008] suggests that baroclinic instabilities in the southern hemisphere can indeed trigger locally intraseasonal variability south of the equator. More studies are needed to determine the possible interaction between these different sources of intraseasonal variability.

[57] Another important conclusion of this paper is the existence, east of 10°W, of an equatorial trapped 15-day variability in SST, that is confined to the Gulf of Guinea, has no signature in SLA and presents no apparent zonal propagation. This variability is observed every summer, with evidence of some interannual variability, and corresponds to the meridional migration, back and forth the equator, of the SST front, north of the equatorial cold tongue. This study shows that variability in meridional wind stress is present throughout the year at comparable periods, between 10 and 20 days, in the eastern equatorial Atlantic. The 15-day variability in SST is thus locally forced by the 15-day variability in meridional wind stress, which excites equatorially trapped mixed Rossby-gravity waves that have maximum meridional velocities along the equator [*Houghton and Colin*, 1987]. The intensity of the SST signature of this 15-day variability is shown to depend strongly on the presence, and intensity, of the seasonal SST front north of the equatorial cold tongue that takes place in boreal summer. Note that the present analysis does not allow to determine if the 15-day variability in SST forces in turn an atmospheric response just above, as it is the case for the tropical instability waves along 2°N west of 10°W [e.g., *Caltabiano et al.*, 2005].

[58] **Acknowledgments.** Support for this study was provided by CNES. The altimeter products were produced by Ssalto/Duacs and distributed by Aviso with support from CNES (http://www.jason.oceanobs.com). TMI data were produced by Remote Sensing Systems and sponsored by the NASA Earth Science REASon DISCOVER Project. TMI data are available at http://www.remss.com. The authors are grateful for the many helpful discussions with Bernard Bourlès, Yves Gouriou and Charly Régnier. They also thank Karina Von Schuckmann for her useful comments on the first version of this manuscript. Comments from two anonymous reviewers have greatly improved the paper.

References

Barnett, T. P. (1983), Interaction of the monsoon and Pacific trade-wind system at interannual time scales. part I: The equatorial zone, *Mon. Weather Rev.*, *111*, 756–773.

Bonjean, F., and G. S. E. Lagerloef (2002), Diagnostic model and analysis of the surface currents in the Tropical Pacific Ocean, *J. Phys. Oceanogr.*, *32*, 2938–2954.

Brandt, P., F. A. Schott, C. Provost, A. Kartavtsteff, V. Hormann, B. Bourlès, and J. Fischer (2006), Circulation in the central equatorial Atlantic: Mean and intraseasonal to seasonal variability, *Geophys. Res. Lett.*, *33*, L07609, doi:10.1029/2005GL025498.

Bunge, L., C. Provost, J. Lilly, M. D'Orgeville, A. Kartavtseff, and J. L. Melice (2006), Variability of the horizontal velocity structure in the upper 1600 m of the water column on the equator at 10°W, *J. Phys. Oceanogr.*, *36*, 1287–1304.

Bunge, L., C. Provost, and A. Kartavtseff (2007), Variability in horizontal current velocities in the central and eastern equatorial Atlantic in 2002, *J. Geophys. Res.*, *112*, C02014, doi:10.1029/2006JC003704.

Caltabiano, A. C. V., I. S. Robinson, and L. P. Pezzi (2005), Multi-year satellite observations of instability waves in the Tropical Atlantic Ocean, *Ocean Sci.*, *1*, 97–112.

Challenor, P. Cipollini, and D. Cromwell (2001), Use of the 3-D Radon Transform to examine the properties of oceanic Rossby waves, *J. Atmos. Ocean. Technol.*, *18*(9), 1558–1566.

Chelton, D. B., F. J. Wentz, C. L. Gentemann, R. A. de Szoeke, and M. G. Schlax (2000), Satellite microwave SST observations of transequatorial tropical instability waves, *Geophys. Res. Lett.*, *27*, 1239–1242.

Chelton, D. B., S. K. Esbesen, M. G. Schlax, N. Thum, M. H. Freilich, F. J. Wentz, C. L. Gentemann, M. J. McPhaden, and P. S. Schopf (2001), Observations of coupling between surface wind stress and sea surface temperature in the eastern Tropical Pacific, *J. Clim.*, *14*, 1479–1498.

Contreras, R. F. (2002), Long-term observations of tropical instability waves, *J. Phys. Oceanogr.*, *32*, 2715–2722.

Düing, W., et al. (1975), Meanders and long waves in the equatorial Atlantic, *Nature*, *257*, 280–284.

Emery, W. J., and R. E. Thomson (2004), *Data analysis methods in physical oceanography*, 2nd ed., 638 pp., Elsevier, Amsterdam, Netherlands.

Foltz, G. R., J. A. Carton, and E. P. Chassignet (2004), Tropical instability vortices in the Atlantic Ocean, *J. Geophys. Res.*, *109*, C03029, doi:10.1029/2003JC001942.

Garzoli, S. L. (1987), Forced oscillations on the equatorial Atlantic basin during the seasonal response of the equatorial Atlantic program (1983–1984), *J. Geophys. Res.*, *92*(C5), 5089–5100.

Garzoli, S. (1992), The Atlantic north equatorial countercurrent models and observations, *J. Geophys. Res.*, *97*(C11), 17,931–17,946.

Grodsky, S. A., J. A. Carton, C. Provost, J. Servain, J. A. Lorenzzetti, and M. J. McPhaden (2005), Tropical instability waves at 0°N, 23°W in the Atlantic: A case study using Pilot Research Moored Array in the Tropical Atlantic (PIRATA) mooring data, *J. Geophys. Res.*, *110*, C08010, doi:10.1029/2005JC002941.

Hashizume, H., S. P. Xie, T. W. Liu, and K. Takeuchi (2001), Local and remote atmospheric response to tropical instability waves: A global view from space, *J. Geophys. Res.*, *106*, 10,173–10,185.

Houghton, R. W., and C. Colin (1987), Wind-driven meridional eddy heat flux in the Gulf of Guinea, *J. Geophys. Res.*, *92*(C10), 10,777–10,786.

Jochum, M., and P. Malanotte-Rizzoli (2003), On the generation of North Brazil Current rings, *J. Mar. Res.*, *61*, 147–173.

Jochum, M., and R. Murtugudde (2006), Temperature advection by tropical instability waves, *J. Phys. Oceanogr.*, *36*, 592–605.

Jochum, M., P. Malanotte-Rizzoli, and A. J. Busalacchi (2004), Tropical instability waves in the Atlantic Ocean, *Ocean Modell.*, *7*, 145–163.

Kummerow, C., W. Barnes, T. Kozu, J. Shiue, and J. Simpson (1998), The Tropical Rainfall Measuring Mission (TRMM) sensor package, *J. Atmos. Ocean. Technol.*, *15*, 809–817.

Lyman, J. M., D. B. Chelton, R. de Szoeke, and R. M. Samelson (2005), Tropical instability waves as a resonance between equatorial Rossby waves, *J. Phys. Oceanogr.*, *35*, 232–254.

Lyman, J. M., G. C. Johnson, and W. S. Kessler (2007), Distinct 17- and 33-day tropical instability waves in subsurface observations, *J. Phys. Oceanogr.*, *37*, 855–872.

Menkès, C. E., et al. (2002), A whirling ecosystem in the equatorial Atlantic, *Geophys. Res. Lett.*, *29*(11), 1553, doi:10.1029/2001GL014576.

Mounier, F., S. Janicot, and G. N. Kiladis (2008), The west african monsoon dynamics. part III: The quasi-biweekly zonal dipole, *J. Clim.*, *21*, 1911–1928.

Peter, A. C., M. Le Hénaff, Y. du Penhoat, C. E. Menkès, F. Marin, J. Vialard, G. Caniaux, and A. Lazar (2006), A model study of the seasonal mixed layer in the equatorial Atlantic, *J. Geophys. Res.*, *11*, C06014, doi:10.1029/2005JC003157.

Philander, S. G. H. (1976), Instabilities of zonal equatorial currents, *J. Geophys. Res.*, *81*, 3725–3735.

Philander, S. G. H. (1978), Instabilities of zonal equatorial currents: II, *J. Geophys. Res.*, *83*, 3679–3682.

Picaut, J. (1983), Propagation of the seasonal upwelling in the eastern equatorial Atlantic, *J. Phys. Oceanogr.*, *13*, 18–37.

Proehl, J. A. (1998), The role of meridional flow asymmetry in the dynamics of tropical instability, *J. Geophys. Res.*, *103*, 24,597–24,618.

Qiao, L., and R. H. Weisberg (1995), Tropical instability wave kinematics: observations from the tropical instability wave experiment (TIWE), *J. Geophys. Res.*, *100*, 8677–8693.

Qiao, L., and R. H. Weisberg (1998), Tropical instability wave energetics: the tropical instability wave experiment, *J. Phys. Oceanogr.*, *28*, 345–360.

Steger, J. M., and J. A. Carton (1991), Long waves and eddies in the Tropical Atlantic Ocean: 1984–1990, *J. Geophys. Res.*, *96*(C8), 15,161–15,171.

von Schuckmann, K. V., P. Brandt, and C. Eden (2008), Generation of tropical instability waves in the Atlantic Ocean, *J. Geophys. Res.*, doi:10.1029/2007JC004712, in press.

Wainer, I., G. Clauzet, J. Servain, and J. Soares (2003), Time scales of upper ocean temperature variability inferred from the PIRATA data (1997–2000), *Geophys. Res. Lett.*, *30*(5), 8004, doi:10.1029/2002GL015147.

Weisberg, R. H., and T. J. Weingartner (1988), Instability waves in the equatorial Atlantic Ocean, *J. Phys. Oceanogr.*, *18*, 1641–1656.

Weisberg, R. H., A. Horigan, and C. Colin (1979), Equatorially-trapped Rossby-gravity wave propagation in the Gulf of Guinea, *J. Mar. Res.*, *37*, 67–86.

Wu, Q., and K. P. Bowman (2007), Interannual variations of tropical instability waves observed by the Tropical Rainfall Measuring Mission, *Geophys. Res. Lett.*, *34*, L09701, doi:10.1029/2007GL029719.

Yu, Z., J. P. McCreary, and J. A. Proehl (1995), Meridional asymmetry and energetics of tropical instability waves, *J. Phys. Oceanogr.*, *25*, 2997–3007.

G. Athie and F. Marin, LEGOS-UMR 5566, CNRS/CNES/IRD/UPS, Centre IRD de Bretagne, BP 70, F-29280, Plouzané, France. (gabriela.athie@ird.fr)